

Energy & Environmental Science

Accepted Manuscript



This is an *Accepted Manuscript*, which has been through the Royal Society of Chemistry peer review process and has been accepted for publication.

Accepted Manuscripts are published online shortly after acceptance, before technical editing, formatting and proof reading. Using this free service, authors can make their results available to the community, in citable form, before we publish the edited article. We will replace this *Accepted Manuscript* with the edited and formatted *Advance Article* as soon as it is available.

You can find more information about *Accepted Manuscripts* in the [Information for Authors](#).

Please note that technical editing may introduce minor changes to the text and/or graphics, which may alter content. The journal's standard [Terms & Conditions](#) and the [Ethical guidelines](#) still apply. In no event shall the Royal Society of Chemistry be held responsible for any errors or omissions in this *Accepted Manuscript* or any consequences arising from the use of any information it contains.

Alkali-metal-enhanced grain growth in $\text{Cu}_2\text{ZnSnS}_4$ thin films†

Cite this: DOI: 10.1039/x0xx00000x

M. Johnson,^a S. V. Baryshev,^b E. Thimsen,^a M. Manno,^a X. Zhang,^a I. V. Veryovkin,^b C. Leighton^{*a} and E. S. Aydil^{*a}

Received 00th January 2012,
Accepted 00th January 2012

DOI: 10.1039/x0xx00000x

www.rsc.org/

The highest efficiency solar cells based on copper zinc tin sulphide (CZTS), a promising photovoltaic material comprised of earth abundant elements, are built on soda lime glass (SLG), a substrate which contains many impurities, including Na and K. These impurities may diffuse into CZTS films during processing and affect film structure and properties. We have investigated the effects of these impurities on the microstructure of CZTS films synthesized by *ex situ* sulfidation of Cu-Zn-Sn alloy films co-sputtered on SLG, Pyrex, and quartz. CZTS films synthesized on SLG were found to have significantly larger grains than films grown on the other substrates. Furthermore, we show that by including a bare additional piece of SLG in the sulfidation ampoule, the grain size of films grown on nominally impurity-free quartz increases from 100's of nm to greater than 1 μm . This demonstrates conclusively that impurities in SLG volatilize in S-containing atmospheres and incorporate into nearby CZTS films synthesized on other substrates. Impurity concentrations in these CZTS films were examined using depth profiling with time-of-flight secondary ion mass spectrometry (TOF-SIMS). Of all the impurities present in SLG, the TOF-SIMS experiments implicated Na, K, and Ca as possible elements responsible for the enhanced grain growth. To investigate the effects of these impurities individually, we introduced very small and controllable amounts of Na, K, or Ca into the sulfidation ampoule during CZTS synthesis. Impurity amounts as low as 10^{-6} moles of Na or 10^{-7} moles of K resulted in a dramatic increase in grain size, from 100's of nm to several microns, for films deposited on quartz, while Ca loading had no visible effect on the final microstructure. Based on this vapor transport mechanism, we thus demonstrate an approach for delivering precisely controlled amounts of specific impurities into CZTS films on arbitrary substrates to facilitate large-grain growth.

Introduction

Copper zinc tin sulfide, copper zinc tin selenide and their alloys $[\text{Cu}_2\text{ZnSn}(\text{S},\text{Se})_4]$ commonly abbreviated as CZTS are sustainable alternatives to copper indium gallium selenide (CIGS) and CdTe as the light absorbing material in thin film solar cells.¹⁻³ The highest efficiency CZTS solar cells are almost always grown on Mo-coated soda lime glass (SLG). This substrate choice is based on three-decades of collective experience with CIGS solar cells, where it was shown that Na readily diffuses from the SLG, through the Mo back contact layer, into the CIGS, thereby increasing the power conversion efficiency.⁴⁻⁹ While the precise mechanisms and fundamental origin of this efficiency enhancement are still debated, it is clear that Na somehow affects the microstructure and carrier concentrations in the CIGS films. To date, very few investigations have focused on precisely how Na influences the microstructure and electronic properties of CZTS. Prabhakar *et al.*¹⁰ and Hliang

Oo *et al.*¹¹ have observed that growing CZTS on SLG or treating a precursor film with an aqueous solution of Na_2S before sulfidation lead to large grains, and Li *et al.*¹² demonstrated that co-evaporating CZTS onto substrates containing Na led to higher hole concentrations, increased carrier mobilities, and improved solar cell efficiencies. In fact, SLG hosts numerous impurities in addition to Na including K, Ca, Mg, and Al. To our knowledge, the effects of these impurities on the microstructure and electronic properties of CZTS films have not been studied systematically.

Herein we present an investigation of the effect of impurities present in SLG on the microstructure of thin CZTS films synthesized through sulfidation of co-sputtered Cu-Zn-Sn alloy films. This investigation revealed that while numerous impurities in SLG can diffuse into the CZTS films, only Na and K diffusion affects the film morphology. Surprisingly, we also found that impurities can be transported through the vapor phase to CZTS films on a

variety of substrates from a piece of SLG placed near the films within the sulfidation vessel. Based on this vapor transport mechanism, we developed an approach for delivering precisely controlled amounts of specific impurities into CZTS films on arbitrary substrates. Using this approach, we investigated the effects of these impurities on grain growth individually. We believe that this controlled impurity introduction method will assist the development of high efficiency CZTS solar cells on substrates other than SLG. Moreover, it will enable controlled studies of the effects of these impurities on electronic properties.

Experimental

CZTS films were synthesized *via ex situ* sulfidation of 430 nm thick Cu-Zn-Sn alloy films. The metallic precursor films were co-sputtered from Cu/Zn (35 at% Cu) and Cu/Sn (60 at% Cu) targets at 10 mTorr using Ar as the working gas with a chamber base pressure of 2×10^{-7} Torr. Precursor films were deposited on SLG, 7740 Corning glass (Pyrex), and z-cut crystalline quartz substrates. Compared to SLG and Pyrex, the quartz substrate is of very high purity and was chosen as a control substrate. The elemental compositions of the SLG and Pyrex substrates were determined using inductively coupled plasma mass spectrometry (ICP-MS) and are presented in Table 1. In addition to Si and O, SLG and Pyrex host a variety of impurities. Within SLG the most prevalent impurity is Na, comprising nearly 9 at% of the glass, followed by Ca and Mg at 4.4 and 3.4 at% respectively, as well as very small amounts of K. Pyrex has a decidedly lower impurity content, with B and Na making up 3.9 at% and 2.6 at% of the glass, respectively.

Table 1. Typical elemental composition of SLG and Pyrex substrates as determined from ICP-MS.

Element	SLG (%)	Pyrex (%)	Element	SLG (%)	Pyrex (%)
Al	0.25	0.52	Na	9.0	2.64
B	0	3.85	P	0.002	0
Ba	0.001	$<10^{-3}$	Si	23.4	28.2
Ca	4.36	0.15	Sr	0.001	$<10^{-4}$
Fe	0.01	0.006	Ti	0.011	0.003
K	0.07	0.008	Zr	$<10^{-3}$	0.013
Mg	3.41	0.004	O	59.5	64.5
Mn	0.01	$<10^{-3}$			

Following deposition, the Cu-Zn-Sn precursor films were sealed in an evacuated quartz ampoule (base pressure of 10^{-6} Torr) with ~ 1 mg of solid S. This ampoule, containing the film and S, was placed in a box furnace and heated at a rate of 6.5 °C/min to 600 °C. The precursor films were sulfidized isothermally at 600 °C for 8 hours before cooling the ampoule back to room temperature naturally. Upon sulfidation, 430 nm thin Cu-Zn-Sn precursor films were transformed into ~ 2.2 μm thick CZTS films. The films were removed by breaking the ampoules and characterized

using a battery of methods including x-ray diffraction (XRD), confocal Raman spectroscopy, scanning electron microscopy (SEM), and energy dispersive x-ray spectroscopy (EDS). Specifically, XRD patterns of sulfidized films were collected using a Bruker D8 Discover system equipped with a Cu $K\alpha$ x-ray source, 0.8 mm beam collimator, and a Hi-Star 2D area detector. Raman spectra were collected at room temperature using a WiTec alpha300R confocal Raman microscope equipped with a UHTS300 spectrometer and a DV401 CCD detector, and the films were illuminated with an Omnichrome Ar ion laser (514.5 nm, ~ 300 nm beam spot size). Raman scattering was collected in a backscattering geometry and dispersed with an 1800 lines/mm grating, resulting in a spectral resolution of 0.02 cm^{-1} . The morphology and spatially averaged elemental composition of the sulfidized films were examined using a JEOL 6500 SEM equipped with a Thermo-Noran Vantage EDS detector. The electron energy was set at 15 keV both for imaging and EDS measurements. At this energy the EDS probe depth is estimated to be near 2 μm , ensuring that the entire depth of the sulfidized films was examined. The average grain size of the CZTS films was determined from SEM images by averaging the number of grains along randomly chosen lines. At least 100 grains were sampled for each film.

The compositional depth profiles were examined using a conventional single-beam approach¹³ time-of-flight secondary ion mass spectrometry (TOF SIMS) in a custom designed instrument (SARISA).¹⁴ The high depth resolution mode available in SARISA was not necessary since the films were very thick with surface roughness approaching nearly 10 % of the total thickness. A 10 keV Ar^+ beam was used in a sequence of alternating cycles that consisted of a direct-current (dc) raster-scanned mode for ion milling followed by a pulsed mode for elemental TOF SIMS analysis with no raster scanning. The Ar^+ beam was produced by an Atomika WF421 ion gun equipped with a Wien filter, raster scan plates, and a pulse generator. The ion gun was inclined at 60° with respect to sample's surface normal. Milling the sample surface in the raster-scanned mode removed surface material from a 500 $\mu\text{m} \times 500$ μm area. Elemental composition information was collected from a 30 μm spot in the centre of the 500×500 μm^2 crater. Every sample was depth profiled at least twice at different locations to ensure reproducibility. TOF SIMS measurements are described in more detail in the Supplementary Information.

The effects of Na, K and Ca on the CZTS morphology were also investigated individually. In these experiments, Na, K, or Ca were charged into the quartz sulfidation tube by coating its walls with aqueous solutions of NaOH, KOH, or $\text{Ca}(\text{OH})_2$. The NaOH solution was diluted from a purchased stock solution, while KOH and $\text{Ca}(\text{OH})_2$ solutions were made by dissolving solid KOH and $\text{Ca}(\text{OH})_2$ in DI water. The amount of NaOH, KOH, or $\text{Ca}(\text{OH})_2$ charge was metered by varying the concentration and volume of the

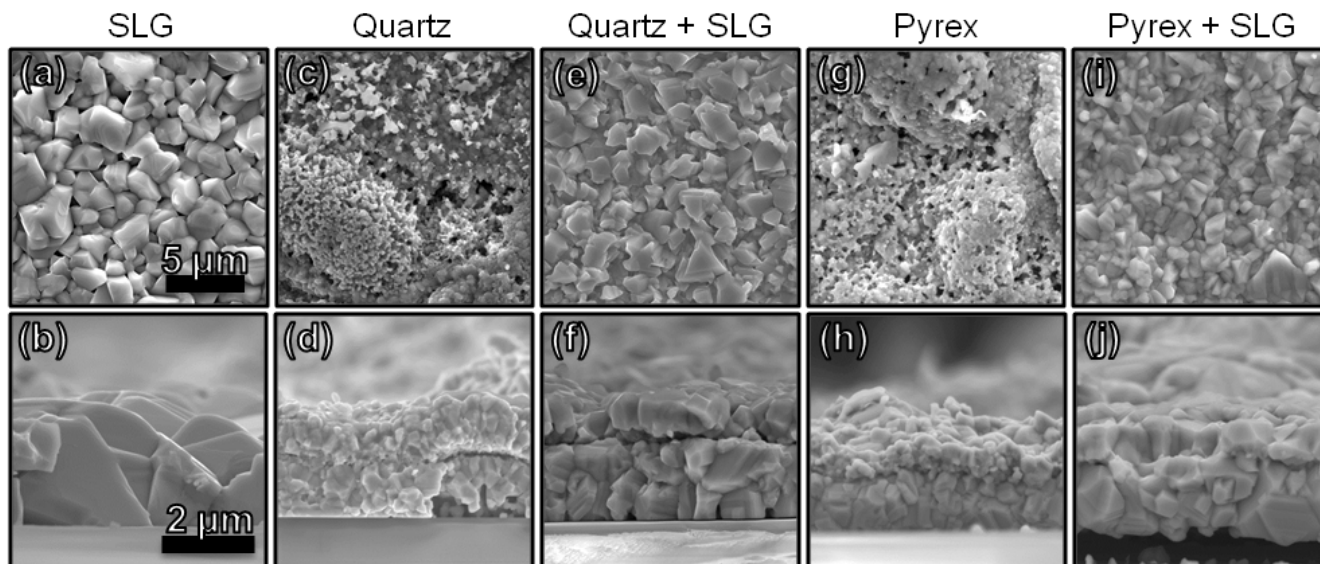


Fig. 1. Plan-view (a, c, e, g & i) and cross-sectional view (b, d, f, h & j) SEM images of CZTS films synthesized through sulfidation at 600 °C, on SLG (a-b), quartz (c-f) and Pyrex (g-j). During the synthesis of films shown in e & f an uncoated piece of SLG was placed in the sulfidation ampoule with the Cu-Zn-Sn films on quartz. Similarly, during the synthesis of films shown in i & j an uncoated piece of SLG was placed in the sulfidation ampoule with the Cu-Zn-Sn films on Pyrex.

solution used to coat the tube walls. Typically 1 mL of solution was added into the quartz tube, and the tube was dried vertically in a convection oven maintained at 100 °C. After the tube dried, the precursor film and S were loaded into the tube and the sulfidation proceeded as described above.

Results and discussion

A detailed study of the evolution of microstructure in films deposited on different substrates revealed a significant surprise. Specifically, we found overwhelming evidence that impurities from the SLG have a remarkable effect on the final grain size. Figure 1 shows plan-view (top row, a, c & g) and cross-sectional (bottom row, b, d & h) SEM images of CZTS films synthesized on SLG (a & b), quartz (c & d), and Pyrex (g & h). A comparison between these SEM images reveals the striking difference in their microstructure. All these films were synthesized under identical conditions, and XRD and Raman spectroscopy indicate that they are all nominally stoichiometric CZTS (*vide infra*).

The CZTS film synthesized on SLG is continuous with an average grain size of $1.38 \pm 0.15 \mu\text{m}$. Essentially, this film is comprised of a monolayer of micrometer size CZTS grains, a highly desirable microstructure for solar cells. On the other hand, films synthesized on quartz and Pyrex have significantly smaller grains. In fact, when viewed from the top, individual grains are not even clearly distinguishable. Cross-sectional SEM images (Figures 1d and 1h) reveal that CZTS films on both quartz and Pyrex have a bilayer structure with grains that do not extend through the entire depth of the film: multiple layers of small grains are visible

through the film thickness. In the film on Pyrex, the layer adjacent to the substrate has a larger, better defined grain structure with an average grain size of $0.47 \pm 0.05 \mu\text{m}$, while the film surface region, (i.e. away from the substrate) has an average grain size of $0.35 \pm 0.03 \mu\text{m}$. Such a difference is not obviously visible in films synthesized on quartz. The layer nearest the substrate in the film on quartz has an average grain size of $0.34 \pm 0.07 \mu\text{m}$, while the surface layer has an average grain size $0.31 \pm 0.04 \mu\text{m}$.

These differences in microstructure could be due to differences in substrate crystallinity, thermal expansion coefficients, or impurity concentrations in the various substrates. To clarify the origins of these differences, we conducted experiments on various substrates to evaluate these possibilities and have concluded categorically that the differences in microstructure and grain size are due to impurities diffusing into the CZTS from the substrate. Firstly, the microstructure of CZTS films found on single crystal quartz is similar to that grown on fused amorphous quartz, which rules out effects due to crystallinity. Secondly, Pyrex and SLG have similar thermal expansion coefficients but the microstructures of CZTS grown on Pyrex and SLG are very different. Finally, two additional experiments, the results of which are also shown in Figure 1, provide unambiguous evidence that impurities are responsible for the larger CZTS grains observed on SLG. In the first of these experiments, identical Cu-Zn-Sn precursor films on quartz were sulfidized with (Figure 1 e & f) and without (Figures 1 c & d) a bare piece of SLG placed in the sulfidation ampoule. The SLG was placed in close proximity to the precursor metal film but the two pieces were not in direct contact. Remarkably, the grain sizes in CZTS films

sulfidized on quartz with this additional piece of SLG in the ampoule are dramatically larger ($1.22 \pm 0.16 \mu\text{m}$, see Figures 1 e & f) than the grain sizes ($\sim 0.3 \mu\text{m}$) in CZTS films sulfidized without the SLG in the ampoule (Figures 1 c & d). A similar result is obtained when comparing Cu-Zn-Sn films deposited on Pyrex, and sulfidized with S alone, (Figures 1 g & h) to CZTS films synthesized on Pyrex with SLG in the ampoule (Figures 1 i & j). A greater than two-fold increase in the average grain size on Pyrex was observed, from $\sim 0.40 \mu\text{m}$ to $0.92 \pm 0.08 \mu\text{m}$, when a piece of SLG was present in the ampoule. Rather surprisingly, it appears that impurities are transported from the SLG substrate placed in proximity to the precursor film, through the vapor phase, to the CZTS film, where they enhance grain growth.

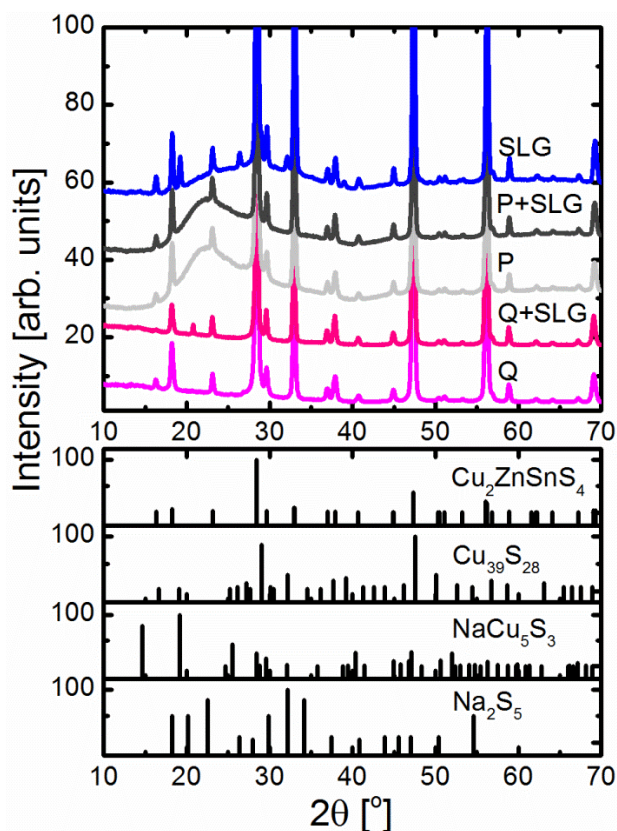


Fig. 2. XRD collected from films sulfidized on SLG, Pyrex and quartz (top panel) at 600°C . The bottom panels show the expected powder diffraction patterns from CZTS and the secondary impurity phases ($\text{Cu}_{39}\text{S}_{28}$, NaCu_5S_3 , and Na_2S_5) encountered in the films for comparison. Q+SLG and P+SLG indicate the films that were synthesized on quartz and Pyrex, respectively, with a bare piece of SLG present in the sulfidation ampoule.

With the exception of the film on SLG, the CZTS films appear to be “phase-pure” within the limits of detection for XRD and Raman spectroscopy. Figure 2 reveals that XRD patterns collected from all the films are consistent with CZTS. The presence of the three CZTS diffraction peaks¹⁵ at 37.0° [(202)], 37.9° [(211)], and 44.9° [(105) and (213)], which are absent in ZnS and very weak in tetragonal Cu_2SnS_3 , confirm the presence of CZTS. Interestingly, the

XRD pattern of CZTS synthesized on SLG also includes weak diffraction peaks at 29.0° , 26.4° , and 19.2° , matching the strongest peak locations of $\text{Cu}_{39}\text{S}_{28}$ (605), Na_2S_5 (012), and NaCu_5S_3 (101), respectively. These phases do not constitute a significant fraction of the sample volume however as their minor diffraction peaks are absent from the XRD pattern. Indeed, we observed infrequent but large grains ($\sim 10 \mu\text{m}$ in size) of impurity phases in plan-view and cross sectional SEM images. These impurity phases appeared to be limited to the surface of the CZTS films, and EDS analysis revealed they contained Na, Cu, S, and Sn, but always lacked Zn.

The Raman spectra from the films displayed in Figure 1 are shown in Figure 3. The major CZTS Raman peak^{16,17} between 333 cm^{-1} and 338 cm^{-1} is present in all the spectra and is accompanied by a broad weaker scattering feature at 288 cm^{-1} that is also characteristic of CZTS films.

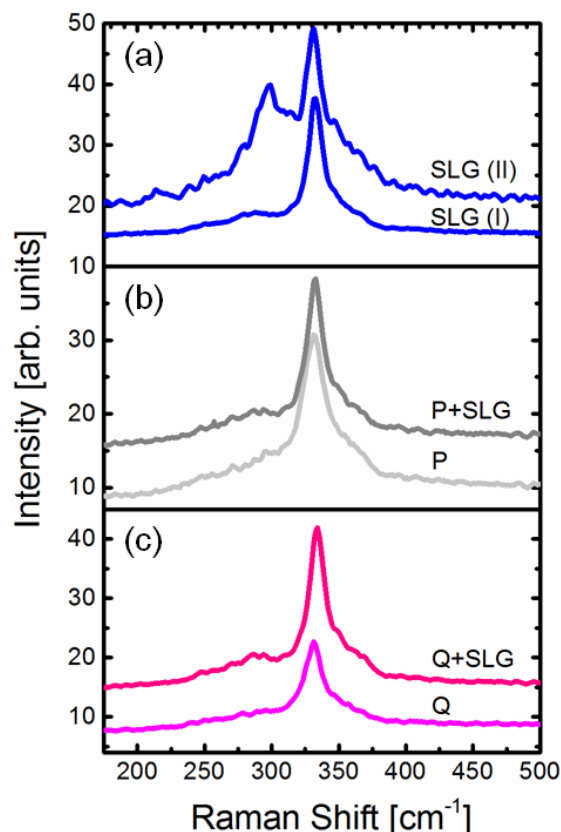


Fig. 3. (a) Raman spectra from two different regions of the CZTS film synthesized on SLG. The spectrum labeled SLG (I) is representative of the majority of the film, while the spectrum labeled SLG (II) was collected from a location on the film where an impurity phase grain was present. Panels (b) and (c) show representative Raman spectra from CZTS films synthesized on (b) Pyrex (P) and (c) quartz (Q), with (P+SLG, Q+SLG) and without (P, Q) a bare SLG present in the sulfidation ampoule.

No other peaks were detected from films synthesized on quartz and Pyrex regardless of whether a bare piece of SLG was present or absent in the ampoule. In contrast, Raman spectra from films synthesized on SLG revealed regions with intense scattering at 297 cm^{-1} (Figure 3, spectrum

labeled SLG II). These regions corresponded to the impurity phases observed with XRD, SEM and EDS. Raman scattering from $\text{Cu}_{39}\text{S}_{28}$ and Na_2S_5 are expected at 474 cm^{-1} and 446 cm^{-1} , respectively.^{18,19} To our knowledge, there is no published Raman scattering data on NaCu_5S_3 . Thus, a possible assignment for the Raman scattering at 297 cm^{-1} is NaCu_5S_3 . The presence of the Na containing impurity phases in films synthesized on SLG is likely due to higher concentrations of Na present in SLG compared to Pyrex and quartz. It is important to note that the films here are synthesized directly on SLG, without a Mo layer. In typical solar cell fabrication, a Mo layer is deposited on SLG as an electrical back contact, which slows and mediates Na diffusion. Lower Na concentrations in films synthesized on Mo-coated SLG compared to films synthesized directly on SLG may be the reason why these impurity phases have not been detected previously.

Table 2 lists the elemental compositions of the CZTS films as determined through EDS. Concentrations of impurities (e.g., K, Ca, Mg, B, etc.) are too low to be accessible with EDS. Moreover, even for the highest concentration impurity, Na, close proximity of its $K\alpha$ peak (1.041 keV) to the $L\alpha$ peak of Zn (1.012 keV) makes compositional quantification difficult and inaccurate.

In order to monitor impurity concentrations below EDS detection limits, we used TOF-SIMS to map the impurity concentration as a function of depth in the CZTS films. During TOF-SIMS measurements, complete mass spectra were recorded at each depth revealing the presence of Na, K, Ca, Mg, B, and Si, albeit at different concentrations.

Table 2. The elemental composition, as determined by EDS, of CZTS films synthesized on (SLG), Pyrex (P) and Quartz (Q) with (P+SLG, Q+SLG) and without (P, Q) an additional piece of bare SLG present in the sulfidation ampoule.

Substrate	Cu(%)	Zn(%)	Sn(%)	S(%)
SLG	25	11	14	50
P	28	11	13	48
Q	27	11	14	48
P+SLG	27	11	14	48
Q+SLG	27	13	13	47

Table 3. The elemental composition, as determined from SIMS intensities and Saha-Eggert analysis, of CZTS films synthesized on (SLG), Pyrex (P) and Quartz (Q) with (P+SLG, Q+SLG) and without (P, Q) an additional piece of bare SLG present in the sulfidation ampoule.

Substrate	Na(%)	K(%)	Ca(%)	Si(%)
SLG	>4	5×10^{-3}	6×10^{-2}	1
P	3×10^{-1}	1×10^{-3}	2×10^{-3}	1
Q	3×10^{-3}	3×10^{-4}	2×10^{-3}	2
P+SLG	1×10^{-1}	6×10^{-4}	5×10^{-3}	5×10^{-1}
Q+SLG	2×10^{-1}	8×10^{-3}	2×10^{-2}	2

Figure 4 shows the profiles of Na, K, Ca, Mg, B, and Si as a function of normalized depth for all CZTS films displayed in Figure 1. The TOF-SIMS intensity for each element is proportional to its local concentration in the film and, hereafter, SIMS intensity and concentration are used interchangeably. We estimated the absolute Na, K, Ca and Si concentrations in the films from the SIMS intensities using the Saha-Eggert approach.^{20,21} The details of this analysis are presented in the Supplementary Information. Table 3 shows the Na, K, Ca and Si concentrations determined from the average SIMS intensities between the surface and $d/d_o=0.4$, where d/d_o is the normalized film depth. The film thickness, d_o , was determined from cross-sectional SEM images (i.e. Figure 1). The location of the CZTS-substrate interface was determined from the significant charging that takes place when the glass substrate is exposed to the sputtering beam and from the ensuing precipitous drop in SIMS intensities. This location corresponds to the normalized depth of $d/d_o = 1$ in Figure 4. The concentrations of Cu, Zn, Sn, and S, the major components of the CZTS film, were nearly identical to each other and were uniform throughout the films' depth (Supplementary Information Figure S2).

The CZTS film synthesized on quartz acts as a control sample for TOF-SIMS characterization since quartz does not contain any of the impurities present in SLG and Pyrex. The impurity levels detected in CZTS films synthesized on quartz thus form the baseline for the TOF-SIMS data collected from films on other substrates. Indeed, for B and Mg, the TOF-SIMS intensities are at the noise level of the instrument. However, we detect Na, K and Ca even in films synthesized on quartz. These elements are ubiquitous and can be incorporated into the CZTS films during any of the steps in the synthesis process. Using the Saha-Eggert method, we calculated that Na, K, and Ca concentrations are 3×10^{-3} , 3×10^{-4} , and 2×10^{-3} at%, respectively.

The Si TOF-SIMS intensity begins to increase at $d/d_o \approx 0.4$ for all films. One possible explanation is that Na diffusion from softening of SLG releases Si into the CZTS. However, we observe similar Si SIMS intensities not only for films on SLG but also for films on Pyrex and quartz. Pyrex and quartz have softening temperatures much higher than $600\text{ }^\circ\text{C}$, yet the SIMS Si intensities in CZTS films on these two substrates are similar to that from the film on SLG. Moreover, quartz is nominally impurity free with no intentionally added Na. This suggests that the Si SIMS intensity is not related to Na diffusion or softening. Instead, we attribute the Si intensity increase beginning at $d/d_o \approx 0.4$ to partial exposure of the substrate to the TOF-SIMS probing beam. This is likely due to a combination of surface roughness and voids within the film, which may be further exacerbated by ion bombardment. Moreover, during the analysis of films synthesized on Pyrex, the depth at which the Si intensity begins to increase is identical to the depth at which the B intensity begins to rise. This is strong evidence

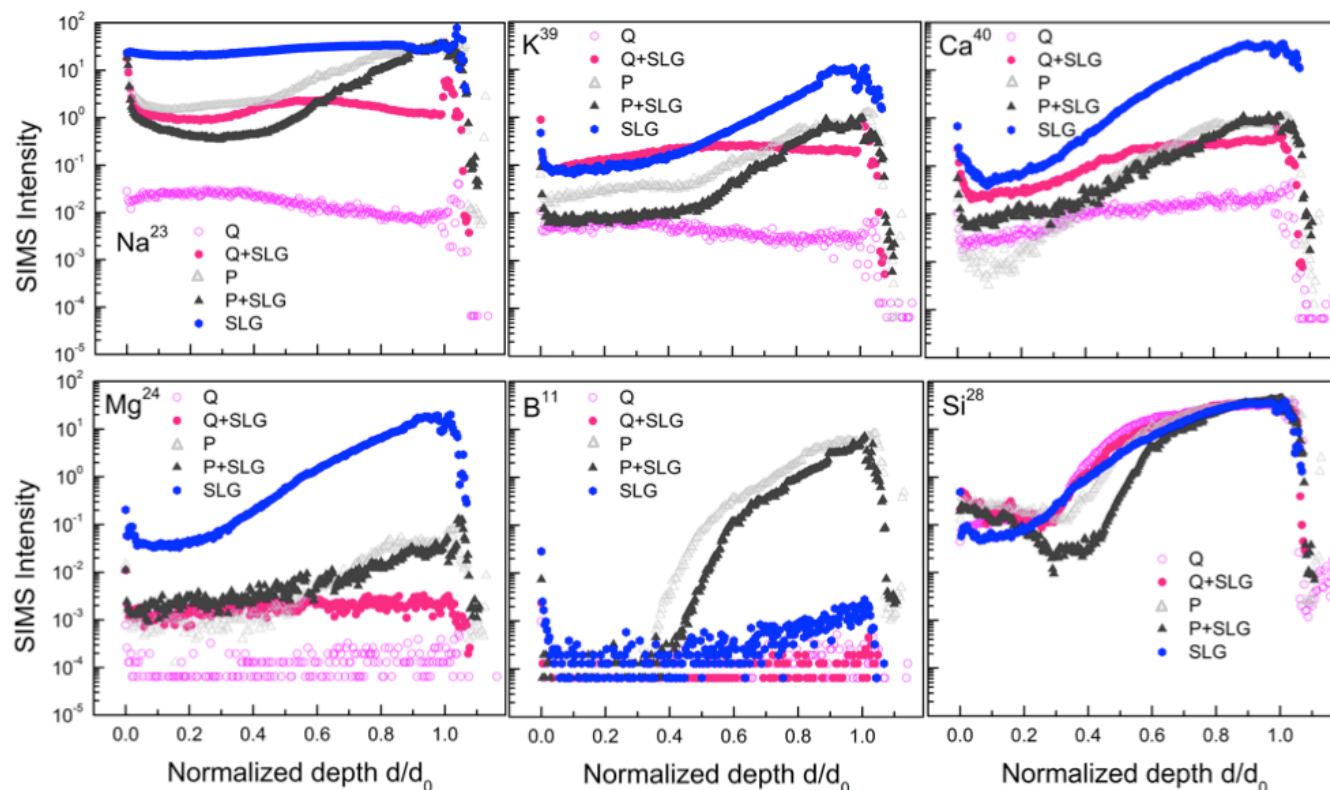


Fig. 4. The TOF-SIMS depth profiles for Na, K, Ca, Mg, B and Si in CZTS films synthesized on soda lime glass (SLG), Pyrex (P) and quartz (Q), with (P+SLG, Q+SLG) and without (P, Q) a bare SLG present in the sulfidation ampoule. The SIMS intensity is shown in counts per primary ion pulse.

that this rise is due to the onset of direct substrate probing by the TOF-SIMS analysis ion beam. Indeed, top view SEM images show that the substrate may be exposed through small voids between the grains.

The Na, K, Ca and Mg concentrations in the CZTS film synthesized on SLG were two to four orders of magnitude higher than those in films synthesized on quartz. Clearly, Na, K, Ca and Mg from SLG easily diffuse into the CZTS films, some of which are responsible for the enhanced grain growth on SLG. In fact, the relative atomic composition of Na is greater than 4 at%, while K and Ca compose 5×10^{-3} and 6×10^{-2} at% of the film, respectively. The significant amount of Na is not entirely surprising since Na containing secondary phases were observed on the surface of this film by EDS and by XRD. The shape of the concentration profile is consistent with the substrate acting as a source for these impurities, with some of the concentration rise after $d/d_0 \approx 0.4$ caused by the substrate exposure to the probing ion beam through the voids between the grains.

The TOF-SIMS concentration profiles of Na, Ca, Mg, and K in CZTS films synthesized on Pyrex are similar to those in films synthesized on SLG, but the SIMS intensities from films on Pyrex are reduced by an amount commensurate with the lower impurity levels found in Pyrex by ICP-MS. The relative percentage of Na, K, and Ca are 3×10^{-1} , 1×10^{-3} , and 2×10^{-3} at%, respectively. These numbers

are considerably higher than those for the CZTS film on quartz. Boron is ruled out as an impurity that can affect the grain size, as the grain sizes of CZTS on Pyrex are small despite the fact that the B concentration is highest in films grown on Pyrex. Additionally, the largest grains are observed on SLG, which contains essentially no B compared to Pyrex.

The CZTS films sulfidized on quartz with an additional piece of bare SLG in the ampoule show significantly elevated concentrations of Na, K and Ca as compared to the CZTS films sulfidized on quartz without the SLG. This remarkable observation confirms that Na, K and Ca are transported via the vapor phase from the SLG to the CZTS film on quartz. In fact, K and Ca concentrations in the film synthesized on quartz with the additional piece of SLG are nearly as high as those in the film synthesized directly on SLG (Table 3). The Na concentrations in the film synthesized on quartz with SLG in the ampoule falls between the Na levels in films synthesized on quartz and on SLG. The Saha-Eggert analysis shows that Na, K, and Ca now make up 2×10^{-1} , 8×10^{-3} and 2×10^{-3} at% of the film respectively. The grain size in films synthesized on quartz with SLG in the ampoule ($1.22 \pm 0.16 \mu\text{m}$) is nearly as large as that in films synthesized on SLG ($1.38 \pm 0.15 \mu\text{m}$) even though the Na concentration in the former is more than one order of magnitude lower than in the latter. This indicates

that even very small amounts of impurities may be effective in enhancing grain growth. The concentration profiles of Na, K and Mg are also nearly flat, which is consistent with these impurities incorporating into the film uniformly from the vapor phase during sulfidation.

With the exception of a few subtle differences, the Na, K, Ca and Mg concentration profiles in the CZTS film sulfidized on Pyrex with an additional piece of bare SLG in the ampoule are very similar to those in the film sulfidized without the SLG. The subtle differences, however, give important insights. First, the Na and K concentration in the film grown on Pyrex without SLG in the ampoule is slightly larger ($\approx 2\times$) than the Na and K concentration in the film grown with the SLG. This is unexpected since SLG provides an additional source of Na and K. Careful examination of Figures 1h and 1j shows that the average grain size in the film grown with SLG in the ampoule ($0.92 \pm 0.08 \mu\text{m}$) is larger than the grain size in the film grown without the SLG ($0.47 \pm 0.05 \mu\text{m}$). This suggests that Na and K may be in the grain boundaries, as a lower Na and K concentration would be expected in the film with the larger grains. Indeed, it is well known that Na in CIGS segregates to grain boundaries.²²⁻²⁴ We also note that high levels of Na and K *within* the film do not necessarily correlate with a coarse-grained microstructure, but it is rather the concentration of Na and K that the film is exposed to during sulfidation that leads to the large grained microstructure. Indeed, the film grown with SLG in the ampoule is clearly exposed to higher impurity concentrations than the film sulfidized without SLG. The increased grain size near the substrate in films on Pyrex sulfidized without SLG also supports this conclusion, as the local concentration of impurities is highest near the substrate-film interface. While Na and K concentration gradients may be expected across the bilayer interface due to small differences in grain sizes, these weak gradients are difficult to observe because they are likely smeared by fluctuations in the position of the interface between the two layers.

We can rule out Mg as the impurity responsible for enhancing the grain growth. The Mg concentration in the film synthesized on quartz with SLG in the ampoule is barely above the noise level (similar to the films grown on Pyrex with or without the additional SLG in the ampoule), and yet the average grain sizes in these films are very different.

In summary, three important conclusions emerge from the experiments discussed so far. First, Na, K, and/or Ca from SLG diffuse into CZTS films and enhance grain growth. Second, the impurities in SLG, particularly Na, K and Ca, are volatilized at 600°C in a S atmosphere and are transported *via* the vapor phase to films placed in close proximity. Third, the *concentration* of impurities that the film is exposed to (*e.g.*, by diffusion from the substrate or from the vapor phase) determines the amount of grain growth, rather than the amount of Na or K within a film itself.

Inspired by the finding that alkali and alkaline earth metals in SLG can be volatilized and transported through the vapor phase, we developed a controlled method to introduce these impurities into CZTS films during sulfidation. Specifically, we introduced Na, K and Ca into CZTS films, one species at a time, by coating the inner walls of the ampoules used for sulfidation with dilute aqueous solutions of NaOH, KOH or $\text{Ca}(\text{OH})_2$. Precise volumes of these solutions were placed in the ampoules and dried to remove water. In this way, metered amounts of Na, K and Ca could

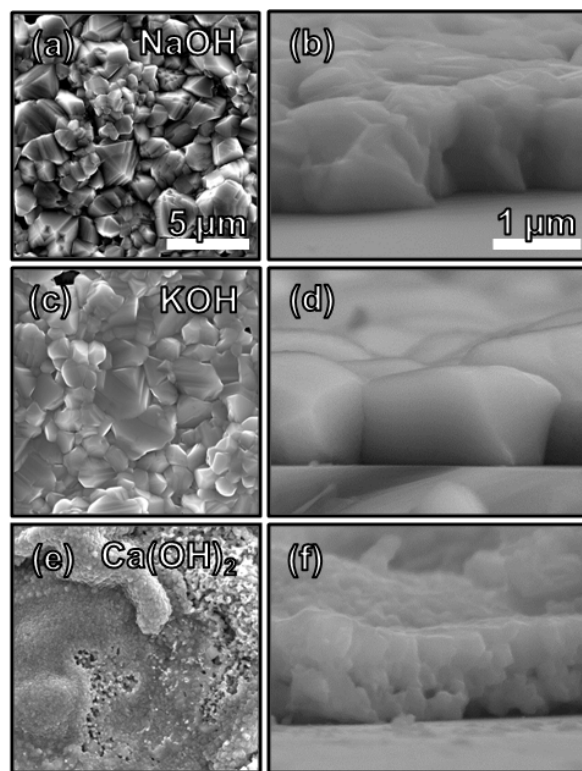


Fig. 5. Plan view and cross-sectional SEM images of CZTS films synthesized on quartz at 600°C with (a & b) $1 \mu\text{mol}$ NaOH, (c & d) $0.1 \mu\text{mol}$ of KOH, and (e & f) $50 \mu\text{mol}$ of $\text{Ca}(\text{OH})_2$ charged into the sulfidation ampoule. The scale bars in a and b apply to all plan view and cross-sectional images, respectively.

be introduced into the sulfidation process. We varied the amounts of Na, K and Ca charged into the sulfidation ampoule over several orders of magnitude. The ranges tested included $95 \mu\text{mol}$ to $0.006 \mu\text{mol}$ of NaOH, $50 \mu\text{mol}$ to $0.003 \mu\text{mol}$ of KOH, and $50 \mu\text{mol}$ to $0.04 \mu\text{mol}$ of $\text{Ca}(\text{OH})_2$. Using this approach, CZTS films were synthesized by sulfidizing Cu-Zn-Sn precursor films on quartz. Indeed, even when small amounts of Na and K were included in the sulfidation ampoule, the grains grew to sizes as large as those observed in films synthesized on SLG. Figures 5a&b, 5c&d, and 5e&f show the SEM images of CZTS films synthesized with $1 \mu\text{mol}$ NaOH, $0.1 \mu\text{mol}$ of KOH, and $50 \mu\text{mol}$ of $\text{Ca}(\text{OH})_2$ charged into the sulfidation ampoule, respectively. Additional characterization data for these films is included in the Supplementary Information (Figures S3-S5). Remarkably, the addition of $1 \mu\text{mol}$ of NaOH or 0.1

μmol of KOH in the sulfidation ampoule resulted in CZTS films with an average grain size of $1.26 \pm 0.10 \mu\text{m}$ or $1.31 \pm 0.18 \mu\text{m}$, respectively. If the charge of NaOH or KOH was too high, the film was no longer continuous and Na and K containing impurity phases dominated the film (Supplementary Information Figure S5). Conversely, if the NaOH and KOH charges were too small, no enhanced grain growth was observed. While the volatile species that transport Na and K to the CZTS film is not known at this time, the vapor pressures of NaOH and KOH are very similar (66.5 and 84.9 mTorr, respectively, at 600 °C), and we thus do not expect this vapor pressure difference could lead to the 10 fold difference in the amounts required to achieve $\approx 1.3 \mu\text{m}$ grains. It appears that K is more efficient in enhancing the CZTS grain growth than Na in terms of impurity charge loading. Note that we did not observe any significant grain growth enhancement with Ca, even though we varied the amount of Ca charged into the sulfidation ampoule between 0.04 μmol and 50 μmol .

These findings raise an obvious question: Precisely *how* do Na and K facilitate grain growth? One obvious possibility is that Na and K may segregate to grain boundaries where they act as fluxing agents that locally lower the melting point. Such lowering of the melting point at the grain boundaries could increase the mobility of the cations, and therefore accelerate grain growth. Another possibility is that Na- and K-containing impurity phases may be acting as intermediates for CZTS formation, thereby accelerating grain growth. The detection of Na- and K-containing phases when films are synthesized with high Na and K concentrations in the sulfidation ampoule suggests that such phases may exist in small amounts during sulfidation, even when the Na and K concentrations are low. These phases are expected to segregate to grain boundaries and may act as high mobility channels for transporting cations from small grains to larger ones during grain growth. Another possibility is that Na and K segregation to the grain boundaries and surfaces alters the surface energy of the CZTS grains making grain growth significantly more energetically favorable. Ineffectiveness of Ca in grain growth enhancement, with the +2 oxidation state as compared to Na and K in the +1 oxidation state, could well be an important observation in this regard. Clearly, elucidating the mechanism of alkali-metal enhanced grain growth remains a challenge and will likely require a careful *in situ* investigation of the grain boundaries and surfaces during growth.

Conclusions

We studied the composition and microstructure of CZTS films synthesized on SLG, Pyrex and quartz through sulfidation of co-sputtered Cu-Zn-Sn metal alloy precursor films. We found that Na and K diffusing from SLG enhanced grain growth during the synthesis of CZTS films. CZTS films with large grains ($>1 \mu\text{m}$) could also be synthesized through vapor transport of Na and K from an

uncoated piece of SLG placed inside the sulfidation ampoule. Inspired by this observation, we developed a method for delivering precisely controlled amounts of Na, K, and other alkali and group II metals to CZTS films during their synthesis. Using this method, we studied and delineated the effects of Na, K and Ca on the microstructure of CZTS films synthesized through sulfidation of Cu-Zn-Sn films. Even 1 μmol of Na was enough to enhance grain growth, and, remarkably, an order of magnitude less K (i.e. 0.1 μmol of K) achieved similar grain sizes.

Acknowledgements

This work was supported partially by the National Science Foundation (NSF) under Award No. CBET-0931145 and partially by the Initiative for Renewable Energy & the Environment, IREE (RL-0004-11). Parts of this work were carried out in the Characterization Facility, University of Minnesota, which receives partial support from NSF through the MRSEC program. E.T. and M. M. were supported by the University of Minnesota NSF Materials Research Science and Engineering Center (DMR-0819885). S.V.B. and I.V.V. were supported under Contract No. DE-AC02-06CH11357 between UChicago Argonne, LLC, and the U.S. Department of Energy (SIMS characterization) and by NASA through grant NNH09AM48I (hardware, testing and optimization of SARISA).

Notes and references

a Department of Chemical Engineering and Materials Science, University of Minnesota, Minneapolis, Minnesota 55455, United States.

b Materials Science Division, Argonne National Laboratory, Argonne, Illinois 60439, United States.

† Electronic Supplementary Information (ESI) available: Additional TOF-SIMS experimental details and additional characterization data. See DOI: 10.1039/b000000x/

- 1 T. K. Todorov, J. Tang, S. Bag, O. Gunawan, T. Gokmen, Y. Zhu and D. B. Mitzi, *Advanced Energy Materials*, 2013, 3, 34–38.
- 2 H. Katagiri, K. Jimbo, W. S. Maw, K. Oishi, M. Yamazaki, H. Araki and A. Takeuchi, *Thin Solid Films*, 2009, 517, 2455–2460.
- 3 I. Repins, C. Beall, N. Vora, C. DeHart, D. Kuciauskas, P. Dippo, B. To, J. Mann, W.-C. Hsu, A. Goodrich and R. Noufi, *Sol. Energ. Mat. Sol. C.*, 2012, 101, 154–159.
- 4 M. Ruckh, D. Schmid, M. Kaiser, R. Schaffler, T. Walter and H. W. Schock, *Sol. Energ. Mat. Sol. C.*, 1996, 41/42, 335–343.
- 5 T. Nakada, D. Iga, H. Ohbo and A. Kunioka, *Jpn. J. Appl. Phys.*, 1997, 36, 732–737.
- 6 L. Kronik, D. Cahen and H. Schock, *Advanced Materials*, 1998, 10, 31–36.
- 7 A. Rockett, *Thin Solid Films*, 2005, 480, 2–7.
- 8 D.-H. Cho, K.-S. Lee, Y.-D. Chung, J.-H. Kim, S.-J. Park and J. Kim, *Appl. Phys. Lett.*, 2012, 101, 023901.
- 9 S. Ishizuka, A. Yamada, M. M. Islam, H. Shibata, P. Fons, T. Sakurai, K. Akimoto and S. Niki, S., *J. Appl. Phys.*, 2009, 106, 034908.

- 10 T. Prabhakar and N. Jampana, *Sol. Energ. Mat. Sol. C.*, 2011, 95, 1001–1004.
- 11 W. M. Oo Hlaing, J. L. Johnson, A. Bhatia, E. A. Lund, M. M. Nowell, M. A. Scarpulla, *J. Electron. Mater.*, 2011, 40, 2214–2221.
- 12 J. V. Li, D. Kuciauskas, M. R. Young and I. L. Repins, *Appl. Phys. Lett.*, 2013, 102, 163905.
- 13 S. V. Baryshev, N. G. Becker, A. V. Zinovev, C. E. Tripa and I. V. Veryovkin, *Rapid Commun. Mass Sp.*, 2013, 27, 2828–2832
- 14 I. V. Veryovkin, C. E. Tripa and M. J. Pellin, *Physics Procedia* 2008, 1, 379–389.
- 15 A.-J. Cheng, M. Manno, A. Khare, C. Leighton, S. Campbell and E. S. Aydil, *J. Vac. Sci. Technol. A* 2011, 29, 051203.
- 16 P. A. Fernandes, P. M. P. Salome and A. F. da Cunha, *Thin Solid Films*, 2009, 517, 2519–2523.
- 17 F. Jiang, H. Shen, W. Wang and L. Zhang, *Appl. Phys. Express*, 2011, 4, 074101.
- 18 P. Kumar and R. Nagarajan, *Inorg. Chem.* 2011, 50, 9204–9206.
- 19 O. El Jaroudi, E. Picquenard, N. Gobeltz, A. Demortier and J. Corset, *Inorg. Chem.*, 1999, 38, 2917–2923.
- 20 C. A. Andersen and J. R. Hinthorne, *Analytical Chemistry* 1973, 45, 1421–1438.
- 21 F. Rüdener, W. Steiger and H. Werner, *Surface Science*, 1976 54, 553–560.
- 22 A. Rockett, J. S. Britt, T. Gillespie, C. Marshall, M. M. Al Jassim, F. Hasoon, R. Matson and B. Basol, *Thin Solid Films* 2000, 372, 212–217.
- 23 D. Braunger, D. Hariskos, G. Bilger, U. Rau and H. W. Schock, *Thin Solid Films* 2000, 362, 161–166.
- 24 D. W. Niles, M. M. Al-Jassim and K. Ramanathan, *J. Vac. Sci. Technol. A* 1999, 17, 291–296.

Copper zinc tin sulfide (CZTS) is an emerging photovoltaic material comprised of earth abundant elements. Presence of very small amounts of sodium and potassium during the synthesis of thin CZTS films enhances grain growth and leads to microstructures ideally suited for solar cells.

